BUDAPEST UNIVERSITY OF TECHNOLOGY AND ECONOMICS
FACULTY OF MECHANICAL ENGINEERING
DEPARTMENT OF POLYMER ENGINEERING

VENCEL PÁL BULMAN

SCIENTIFIC STUDENT'S ASSOCIATIONS RESEARCH
INVESTIGATION OF THE ENERGY ABSORPTION CAPABILITY AND DESIGN OF A CARBON FIBER REINFORCED COMPOSITE CRASH STRUCTURE

Supervisor:
Bence Szederkényi
PhD student

BUDAPEST, 2023

ACKNOWLEDGEMENTS

The project supported by the Doctoral Excellence Fellowship Programme (DCEP) is funded by the National Research Development and Innovation Fund of the Ministry of Culture and Innovation and the Budapest University of Technology and Economics, under a grant agreement with the National Research, Development and Innovation Office.

The research reported in this paper was supported by the National Research, Development and Innovation Office (NRDI, Hungary) through grants OTKA FK134336 and OTKA K 138472.

Project no. TKP-6-6/PALY-2021 has been implemented with the support provided by the Ministry of Culture and Innovation of Hungary from the National Research, Development and Innovation Fund, financed under the TKP2021-NVA funding scheme.

Project no. 2022-2.1.1-NL-2022-00012 „National Laboratory for Cooperative Technologies" has been implemented with the support provided by the Ministry of Culture and Innovation of Hungary from the National Research, Development and Innovation Fund, financed under the National Laboratories funding scheme.

TABLE OF CONTENTS

LIST OF NOTATIONS

Latin characters

Notation	Description, note, value	Unit
EA	Young's modulus in 1-direction	GPa
EB	Young's modulus in 2-direction	GPa
DFAILC	Maximum strain for fiber compression	-
DFAILM	Maximum matrix tensile/compressive strain	-
DFAILT	Maximum strain for fiber tension	-
GAB	Shear modulus	GPa
PRBA	Minor Poisson's ratio	-
SC	Shear strength	MPa
XC	Compressive strength in 1-direction	GPa
XT	Tensile strength in 1-direction	GPa
YC	Compressive strength in 2-direction	MPa
YT	Tensile strength in 2-direction	MPa

Greek characters

Notation	Description, note, value	Unit
θ	Fiber orientation angle	°

Abbreviations

Abbreviation	Description
CFE	Crush Force Efficiency
CFRP	Carbon fiber reinforced polymer
IA	Impact Attenuator
UD	Unidirectional
SEA	Specific Energy Absorption

1. INTRODUCTION

Fiber reinforced polymer matrix composite materials are widely applied owing to their outstanding specific properties. They provide enhanced stiffness, strength, corrosion- and fatigue resistance compared to metals and are meant to replace them in weight-critical components in engineering fields such as aerospace and motorsport. This mainly applies to fiber reinforced composites, which consist of fibers such as carbon, glass or aramid embedded in a polymer matrix such as epoxy, polyester, or vinyl ester.

One of the more specific applications of composites is their use in crash structures. Traditional metallic components absorb energy through plastic deformation, which composites are not capable owing to the lack of ductility of the fibers. Instead of plastic deformation, the most efficient energy absorbing mechanism of composites is (properly initiated) crushing, which involves the fragmentation of the reinforcement fibers. When designed properly, this form of failure has the potential to be more effective than the plastic deformation of metallic parts, while reducing the weight of the component. The amount of absorbed energy depends on the geometry, material properties and orientation, and the crushing initiation mechanism.

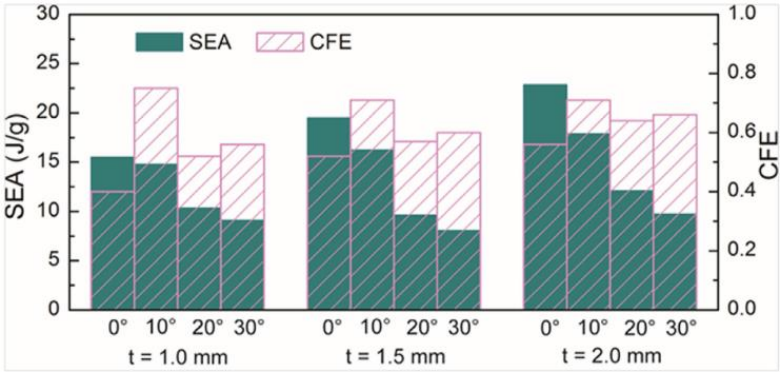

Fig. 1: Comparison of SEA (Specific Energy Absorption) and CFE (Crush Force Efficiency) of aluminium tubes with different thicknesses under different loading angles [25]

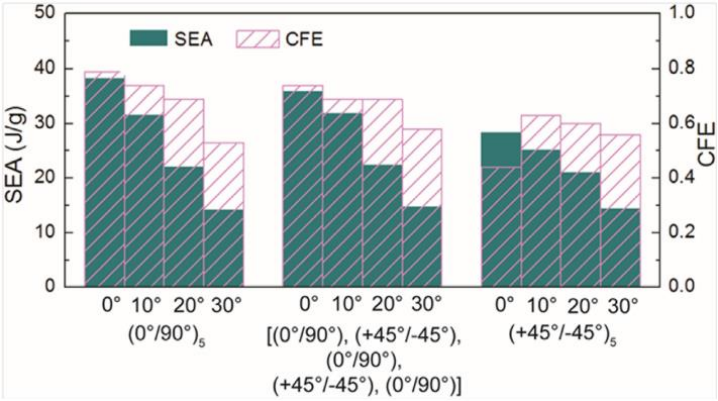

Fig. 2: Comparison of SEA (Specific Energy Absorption) and CFE (Crush Force Efficiency) of CFRP tubes with different layups under different loading angles [25]

The goal of this study is to determine the ideal parameters for a crash structure designed with the rules of the Formula Student collegiate competition in mind. The design process involves both the determination of material properties through material testing and the use of these properties as inputs for FE simulations. The simulation model will be validated through this testing so that complicated geometries can be analyzed without the need for physical specimens, which would incur additional costs and time.

2. LITERATURE REVIEW

The goal of this section is to collect information on the failure and crashworthiness characteristics of fiber-reinforced composite materials.

2.1. Failure of composite materials

Fiber-reinforced composite materials are made up of two (or more) constituent materials. This study focuses on fiber-reinforced polymer (FRP) composites, which consist of load-carrying fibers and a polymer matrix, which embeds the fibers and acts as the load-carrying constituent. To achieve the load transfer between the fibers, strong adhesion is required at the fiber-matrix interface [23].

One of the limitations of composites is the difficulty of modeling their failure properties characteristics. Fig. 3 outlines some important parameters which define the mechanical properties of a composite structure [23].

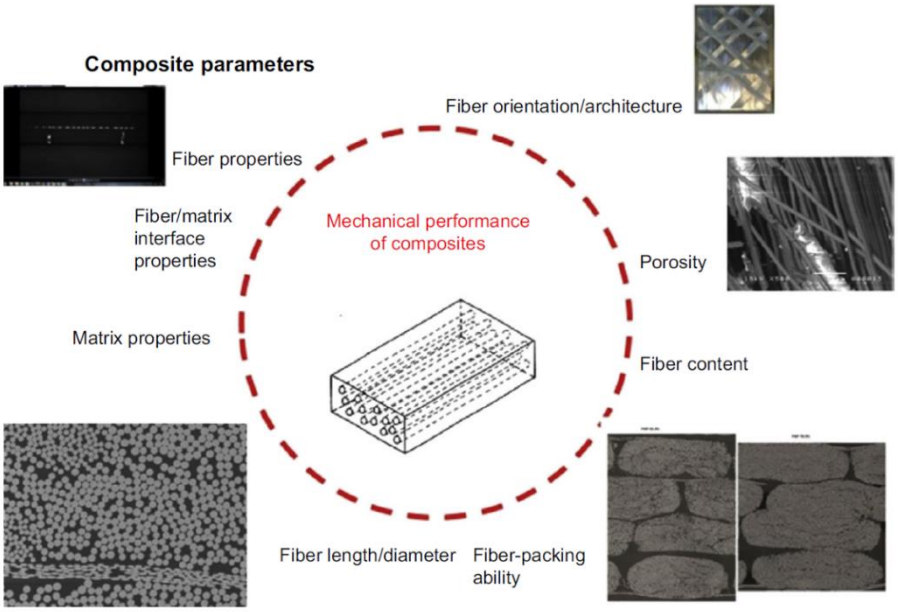

Fig. 3: Parameters with a defined effect on the mechanical properties of composites [23]

The drawback of multi-phase materials is the lack of homogenous material behavior and the possibility of multiple failure modes. The material and failure can also be observed at multiple scales, ranging from microscopic to macroscopic, with no existing unified approach. The most common practice is to observe the material at the meso-scale, a compromise between micro-scale (separate fiber and matrix) and macro-scale (homogenous laminate) modeling. Meso-scale modeling treats each lamina as a separate entity, enabling the investigation of interlaminar properties. This approach provides a considerably better model of material behavior than the macro-scale method while also being computationally cheaper than the micro-scale approach [33].

Fig. 4 shows the possible load cases which can lead to the damage and failure of composite structures: fracture occurs in tension (A, C), compression (B1, B2, D) or shear (E, F, G) parallel or normal to the fiber direction [24].

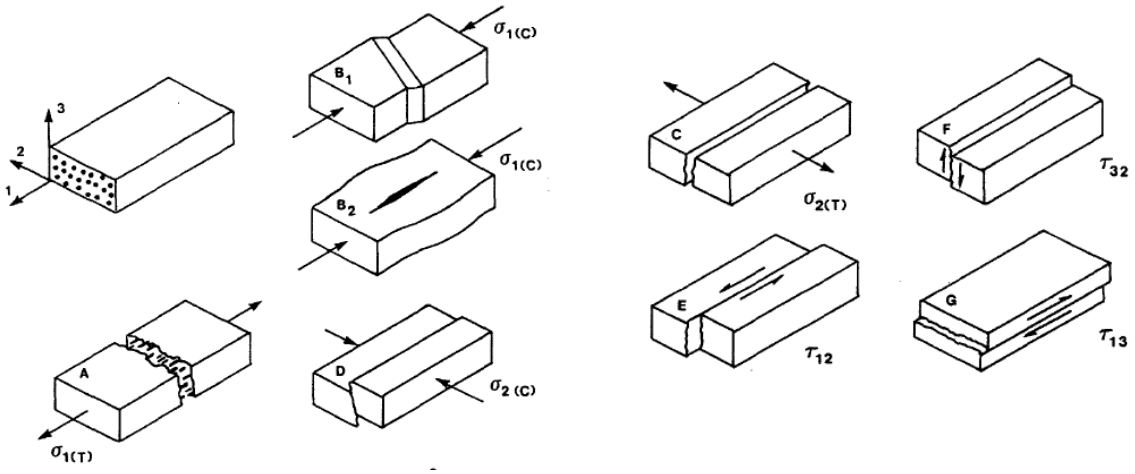

Fig. 4: Fracture modes of a unidirectional fibre composite lamina; A: parallel tension; B1, B2: parallel compression; C: normal tension; D: normal compression; E, G: parallel shear; F: normal shear. [24]

The generic damage mechanisms that can occur as a result of these load cases are discussed in the following chapters.

2.1.1. Fiber-matrix debonding

Occurs due to loading perpendicular or parallel to the fiber direction. The former is more common, being caused by the difference in the stiffnesses of the fiber and matrix. The latter is mostly associated with fatigue loading. Fig. 5 shows multiple debonds caused by perpendicular loading forming a crack [23].

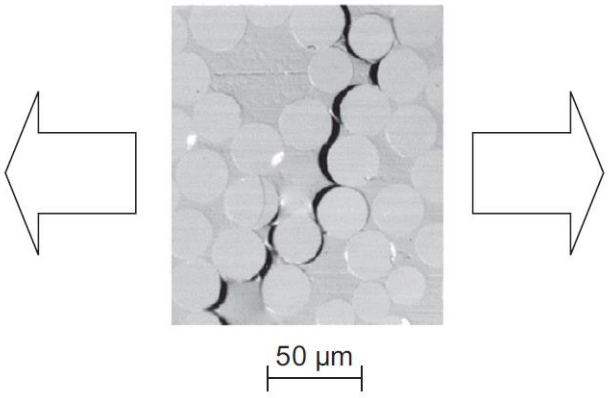

Fig. 5: Crack formed as a result of fiber-matrix debonding [23]

2.1.2. *Fiber fracture*

The properties of fibers are influenced by the diameter, defects introduced during fiber/ composite manufacture. This means that nominally identical fibers in a bundle will not have identical mechanical properties, including failure limits. As a consequence, the stress concentration caused by isolated cases of fiber fracture can induce failure in adjacent fibers, as seen on Fig. 6 [23].

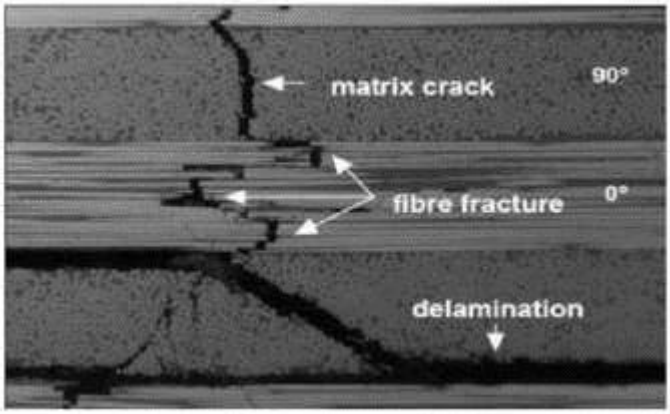

Fig. 6: Fiber fracture in carbon composites [34]

2.1.3. *Matrix cracking*

Matrix cracks usually extend across the thickness of the ply, often initiating at the free edges of a test specimen. The extent of the damage caused by cracks that extend across the width of a planar specimen is quantified as cracks per unit length of specimen (crack density, D). When the cracks are discontinuous, cracked area per unit volume is used [23].

Crack onset (fast fracture, means a rapid growth of cracks) usually occurs around 0.4-0.6% strain. Splitting is a type of matrix cracking where the crack runs parallel to the direction of the applied load. Its cause is the mismatch in the Poisson ratio between adjacent. Splits can either grow by fast fracture or as fatigue cracks. An example of splitting can be seen on Fig. 7 at the 1.69% strain specimen [23].

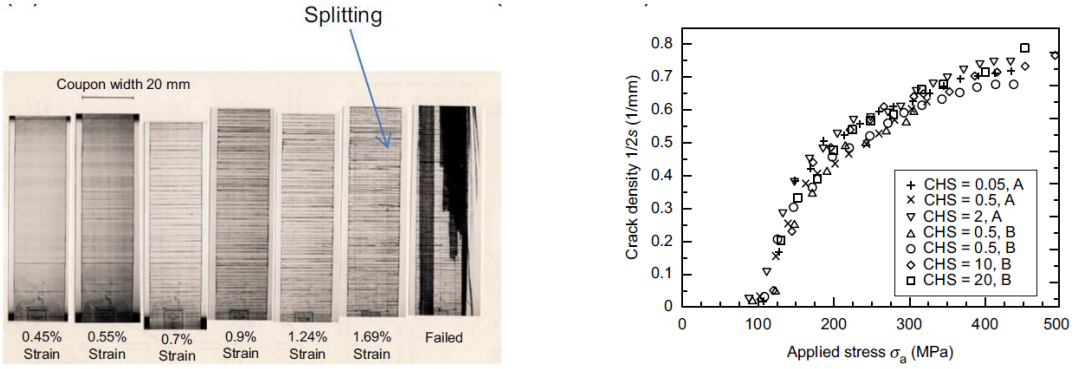

Fig 7: (a) Matrix cracking at different strains and (b) crack density as a function of stress [23]

2.1.4. Delamination

Delaminations are a result of a mismatch in elastic properties between adjacent plies. It occurs as a result of peel and shear stresses at a free edge and the presence of a matrix crack. An example of delamination at the interface of a 90° and +45° ply is shown on Fig. 8 [23].

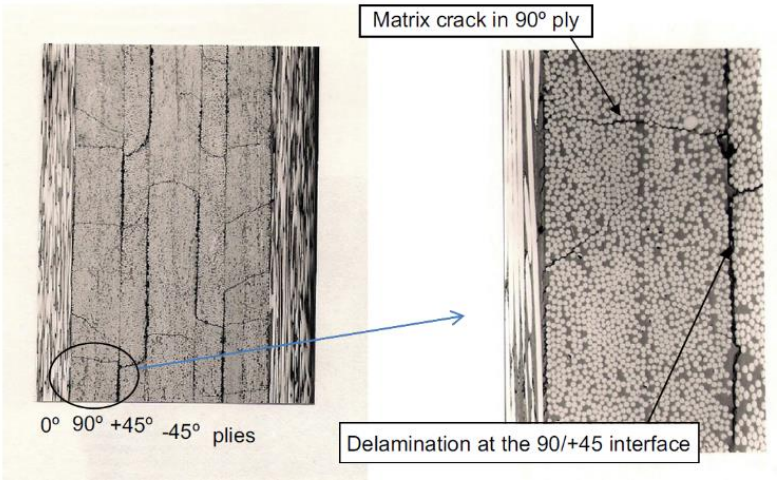

Fig 8: Delaminations between plies with different orientations [23]

2.2. Crashworthiness characteristics of composite structures

Vehicle crash structures are meant to reduce the impact of the collision on the passengers through energy dissipation. This process results in the deformation of the compartment, which means that the definition of safe design criteria is critical. These criteria can be in the form of a limit on force transmission or deformation. The mechanical elements absorbing the impact do so through axial crushing, bending and/or combined loading [1].

Composites are generally applied as thin-walled structures (tubes, profiles, cones) subjected to axial crushing. The energy absorption is a result of the properly initiated, stable and controlled crushing of the material which involves the fragmentation of the reinforcement fibers, as opposed to metallic components which absorb energy by plastic deformation [1]. The bending crush behavior is not in the scope of this study.

The most important characteristic of the event and the accompanying load-displacement curve as shown on Fig. 9 are the following:

- Absorbed energy: Its magnitude is equal to the area under the load-displacement curve
- Peak load: The maximum load during the event
- Post crushing region: The area of the load-displacement curve past the peak load
- Specific energy absorption: absorbed energy related to the mass of the component [1].

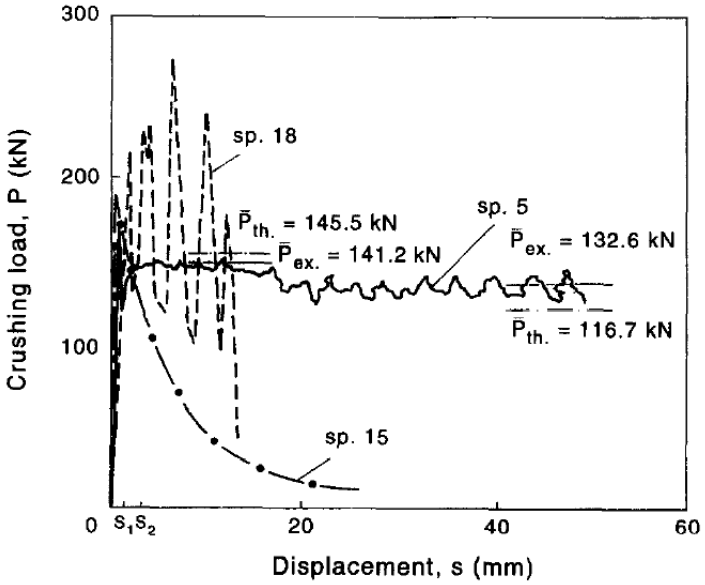

Fig. 9: Load-displacement curves for hourglass rail shells subjected to static and dynamic loading for various collapse modes. Mode I static (sp.5), Mode II. static (sp.15), Mode I dynamic (sp. 18) [l].

The main parameters influencing the crashworthiness of composite structures are discussed in the following points.

2.2.1. Material

Experimental characterization of the material properties through testing and with a variety of loads is necessary to understand the material response. Since composites consist of two constituent materials, it might be required to also characterize them

separately. The orientation of the fibers, fiber content and mechanical properties also influence the energy absorption capability of the structure [1].

Fiber

The most used reinforcement materials for composite energy absorbing structures are carbon, glass and aramid fibers, usually combined with a thermoset resin such as epoxy. Based on tests conducted by Thornton [3] and Farley [4], carbon-epoxy tubes perform better than ones made of glass-epoxy or aramid-epoxy. Tests have also been conducted for hybrid composites, which combine the properties of multiple fibers. Farley reports that the energy absorption of these specimens was not significantly better, with Thornton and Edwards [5] reporting the presence of aramid fibers in combination with carbon and glass leads to unstable collapse by folding. Within a single-fiber system, the failure strain of both the matrix and fiber determine the energy absorption capability, with higher values providing better energy absorption.

Matrix

For the energy absorption to be as effective as possible, the failure strain of the matrix should be higher than that of the fibers [1]. In addition to thermoset matrices, thermoplastic materials are also successfully applied for this application, as demonstrated by Hamada et al. [6]. The use of thermoplastic polyetheretherketone (PEEK) provided double the energy absorption compared to epoxy, both being combined with carbon fiber. The crack resistance of the PEEK matrix is primarily responsible for this result.

Laminate design

The ply orientations in a layup have a considerable effect on the energy absorbing capability of a composite structure [1]. Farley [4] performed quasi-static tests on [0/± θ] carbon-epoxy tubes, with the ply orientation angle θ ranging from 0° to 45°. The 0° direction is the axial direction of the tube. The results indicate that the absorbed energy decreases with increasing θ. Circular tubes (Fig. 10) made of [0/± θ] glass-epoxy and [0/± θ] aramid-epoxy also showed variations with θ ranging from 45° to 90°. The energy absorption capability increased with increasing θ. Schmueser and Wickliffe [7] performed dynamic drop tower tests without the use of a collapse trigger mechanism (see later) for stable collapse initiation. They reported differing results, with the energy absorption capability of [0_2/± θ] carbon-epoxy, aramid-epoxy and glass-epoxy specimens increasing with increasing θ.

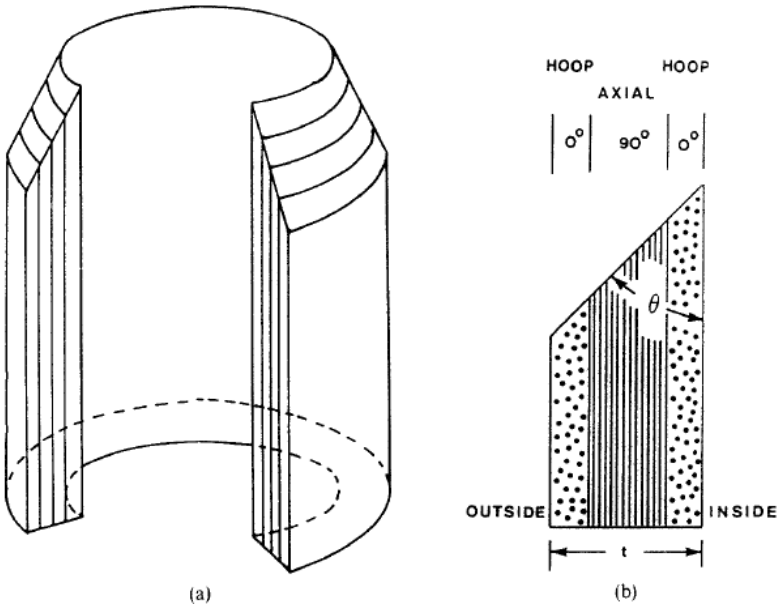

Fig. 10: Schematic of a (0/90/90/0) chamfered composite tube. (a) Section of the tube; (b) Geometry and chamfer trigger [24].

2.2.2. Geometry

Several studies have been carried out to investigate the effect of the geometry of thin-walled composite structures on their energy absorbing capability. These include the wall thickness t, axial length L, and diameter D. Frusta (pyramid or cone cut with a plane parallel to the base) are also examined with an additional parameter: semi-apical angle [1].

Circular tubes

Circular tubes (Fig. 5) are generally the most effective geometry for energy absorption, since there are no stress concentration points as opposed to square or rectangular specimens. This is reported by both Thornton and Edwards [5] and Mamalis et al. [8].

Farley [9] reports that the energy absorption of circular tubes is a non-linear function of the ratio D/t (diameter/thickness), with energy absorption falling as D/t increases. These tests were performed on $[\pm 45]_n$ carbon-epoxy and aramid-epoxy tubes. In the case of carbon-epoxy tubes, the non-linear dependence on D/t varied with different internal diameters, while aramid-epoxy specimens didn't show this property. This points to the fact that aramid-epoxy tubes can be scaled for energy absorption by changing the diameter, as opposed to carbon-epoxy tubes. As for the thickness of the tube, Mamalis et al. [10] investigated glass-polyester tubes and used the tube slenderness ratio t/D as a parameter of the total absorbed energy W. The absorbed energy increased with an increasing t/D ratio.

Square/ rectangular tubes

Tubes with a square or rectangular cross section are less effective at absorbing energy as reported by multiple studies [5, 8]. The most obvious reason for this is the fact that the corners act as stress concentration points and lead to splitting cracks [1]. Mamalis et al. [8] also report that the energy absorption of axially loaded square tubes is independent of axial length.

The choice of trigger geometry for stable collapse also affects the energy absorbing capability. According to Czaplicki et al. [11], tubes with bevel triggers performed worse than those with tulip triggers, which also had the benefit of a more controlled and stable collapse mechanism. The subjects of their experiments were E-glass/polyester and E-glass/ vinyl ester pultruded tubes.

Conical shells

Conical shells do not require a separate collapse trigger mechanism in order to ensure a stable and controlled collapse. The most important geometric parameter is the semi-apical angle of the frusta, which several studies have observed [12-15]. It has been concluded that specific energy absorption decreases with increasing semi-apical angle. The transition point between stable and unstable collapse has been observed to be around 15-20° [14, 15]. Frusta with circular and square cross sections were compared by Mamalis et al. [13], with the study concluding that circular cross sections are more effective at observing energy.

Other geometries

Non-conventional geometries have also been subjects of past studies, including an hourglass cross-section, observed by Mamalis et al. [8]. The study concluded that this shape has better specific energy absorption than square tubes. The energy absorption stays nearly constant with an increasing ratio of t/L (thickness/axial length), meaning that the axial length of the tube has no significant effect on the crashworthy capability of the structure.

Near-elliptical carbon-epoxy tubes were studied by Farley and Jones [16]. The elliptical shape was produced by two identical parts of a circular tube with their centers of curvature offset. The study concluded that the greater this offset was (resulting in a more 'elliptical' shape), the greater the energy absorbing capability of the structure. Examples of hourglass and near-elliptical geometries can be seen on Fig. 11.

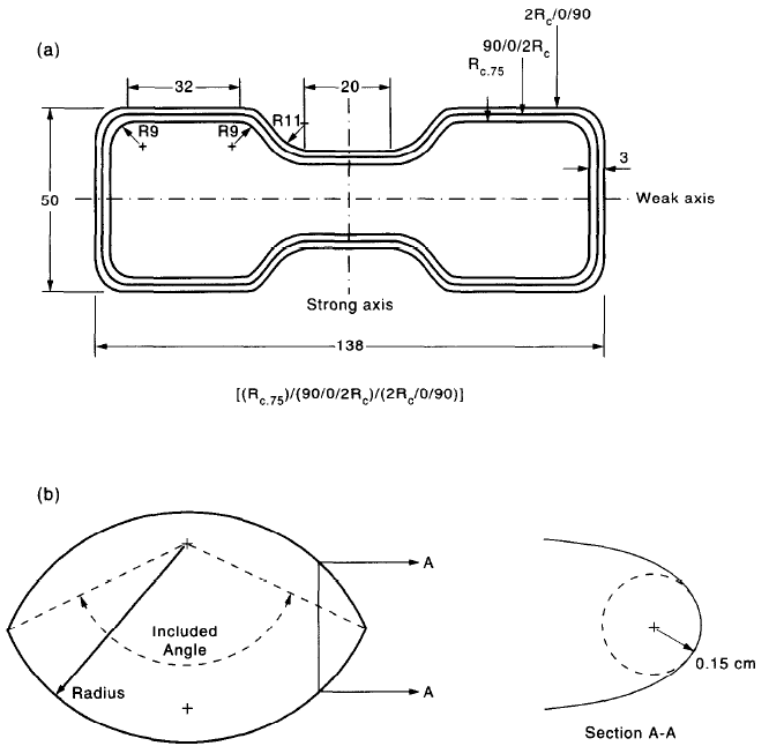

Fig 11: (a) Cross-section of a rail beam [26] and (b) a 'near-elliptical' shell [16]

2.2.3. Loading conditions

The effect of static and dynamic axial loading on energy absorption has been widely researched. The dependence of energy absorption on crushing speed – strain rate – is the result of the mechanisms of the crushing process, which may be strain rate dependent. The effects of strain-rate can generally change the behavior of the fiber and matrix, in addition to modifying the coefficient of friction between surfaces sliding on each other during the crushing process [1].

A study by Farley [17] subjecting carbon-epoxy and aramid-epoxy specimens to constant crushing speeds ranging from 0,01 m/s to 12 m/s concluded that the strain-rate can influence the stiffness and failure strain of the matrix, while the properties of brittle fibers remained unchanged. The $[\pm\theta]_3$ carbon-epoxy specimens showed an increase in energy absorption up to 35% over the tested speed range, while the $[0/\pm\theta]_2$ specimens showed no sensitivity to crushing speed. The value of θ took on the values 15°, 45° and 75° in all tests. All aramid-epoxy specimens showed strain-rate sensitivity, with energy absorption increasing between 20-45% over the crushing speed range. It may be assumed that in case of the $[0/\pm\theta]_2$ carbon-epoxy specimens, the fibers control the crushing process, which is why the tubes show little to no crushing speed sensitivity [1].

The friction mechanisms between the various surfaces formed during the crushing process are also affected by crushing speed as shown by Mamalis et al. [8, 12, 13]. They also concluded that energy absorption values during dynamic collapse are lower than

for static tests performed on thin-walled fiberglass-polyester tubes of varying geometries (circular, square tubes and frusta). This is supported by Schmueser and Wickliffe [7], who conducted static and dynamic tests on $[0/\pm\theta]_2$ carbon-epoxy, glass-epoxy and aramid-epoxy specimens and reported that the dynamic specific energy is lower for all three composite materials. Kindervater [18] notes that the choice of material system has a considerable effect on the results, demonstrated on carbon-epoxy, polyethylene (Dyneema SK60) – epoxy, and carbon - (thermoplastic) polyamide material pairings tested at speeds up to 9 m/s. The carbon-epoxy specimens showed a 20% degradation at the highest speed, while the rest of the specimens showed improvements nearing 50%.

The studies highlighted above were all conducted on tube specimens, which are not always representative of real structures. As demonstrated by Savage [19], the failure mechanism of a Formula 1 composite nose cone subjected to quasi-static loading did not match the progressive failure outlined in the literature above.

2.3. Failure mechanisms of dynamically loaded composite structures

2.3.1. Microfracturing

Failure initiation begins at the microscale and determines the macroscopic failure mode of the structure. The most common microscopic failure modes are discussed in Chapter 2.1, including fiber fracture, matrix cracking, fiber pullout and fiber-matrix debonding. The goal of the crushing process is to enable stable collapse, meaning the specimen can support compressive loads even following local damage, as opposed to unstable failure which is characterized by a drop-off in load bearing capability after an initial spike [1].

Microscopic processes could lead to one of four basic macroscopic crushing modes identified by Farley and Jones [20] in tubes subjected to axial loading: transverse shearing, local buckling, lamina bending and brittle fracture (discussed in detail in Chapter 2.3.2). Brittle fiber composites exhibit lamina bending and transverse shearing crushing modes (or a combination of both), while ductile and select brittle fiber-reinforced composites exhibit local buckling [1].

The main microscopic process influencing the crushing mode is the length of the inter/intralaminar cracks formed during load application on the crushing initiator. The transverse shearing crushing mode is characterized by interlaminar and longitudinal cracks which are shorter than the length of the laminate, while the cracks formed during lamina bending are long (generally 1-10 laminate thicknesses) inter/intralaminar and parallel-to-fiber cracks [1].

As for local buckling, it characterizes the failure of ductile fibers capable of plastic deformation for the formation of local buckles. Brittle fiber-reinforced composites can

also exhibit local buckling in case the interlaminar stresses are small enough relative to the strength of the matrix, the failure strain of the matrix is higher than that of the fiber, or the plastic deformation is provided by the matrix (as opposed to the brittle fibers) [1].

Generally, the crushing modes are each controlled by different microscopic mechanisms: transverse shearing is dependent on interlaminar crack growth and lamina bundle fracture; lamina bending on inter/intralaminar crack growth and friction; and local buckling on plastic yielding of fiber/matrix [1].

2.3.2. Macroscopic collapse modes

Thin-walled composite tubes subjected to axial loading absorb energy through multiple macroscopic failure modes. The four stable collapse modes identified by Farley and Jones [20] serve as the basis for this topic and are often quoted in literature [30, 31, 32]: fiber splaying, fragmentation, brittle fracture and local buckling. The first three are more relevant in terms of the energy absorption of composites and are shown on Fig. 12 [30].

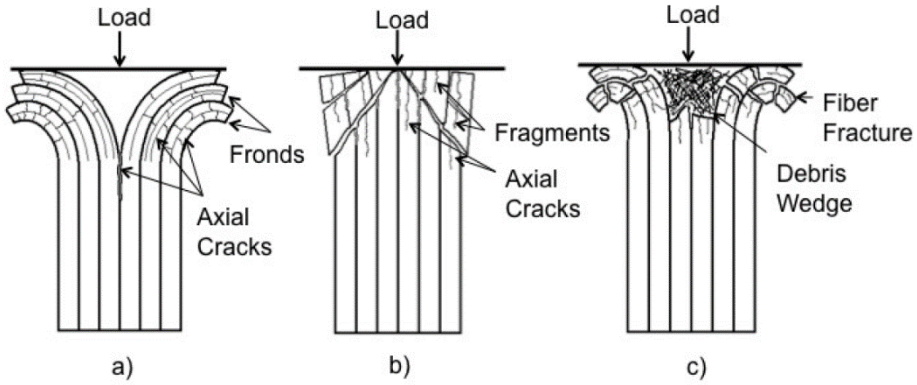

Fig. 12: (a) Fiber splaying, (b) fragmentation and (c) brittle fracture [30]

Fiber splaying / lamina bending

This failure mode is characterized by the fiber bundles or fronds (Fig. 13b) which are separated by the interlaminar, intralaminar and axial cracks which are longer than the laminate thickness, as outlined in Chapter 2.3.1. The load platen then deforms these fronds at a curvature radius and forces them inside / outside the tube wall. During this process – and the delamination of the tube wall – shear and tensile stresses develop in the composite, which can cause Mode I and Mode II fracture. The fronds experience some extent of fracture, an excessive amount points to the presence of fragmentation and brittle fracture (Fig. 12) as a result [30].

Another characteristic of the crush zone is the debris wedge (Fig. 13c), which forms during the development of stable mechanisms during the initial stages of the process.

This mechanism has been studied in detail by Fairfull and Hull [21] and Mamalis et al. [2, 10, 22] among others.

The main features of the fracture mechanisms of axially loaded square and hourglass section tubes are described by Mamalis et al. [2] and are representative of a general splaying mode crush zone (Fig. 13) [1].

1. Annular wedge of fragmented material forced through the shell wall.
2. Intrawall microcrack ahead of the crush zone ahead of the apex of the annular wedge.
3. Internal and/or external fronds created as a result of the delamination caused by the central bundle wedge.
4. Compressive-tensile strained zone between the central crack and the shell wall edges [1].

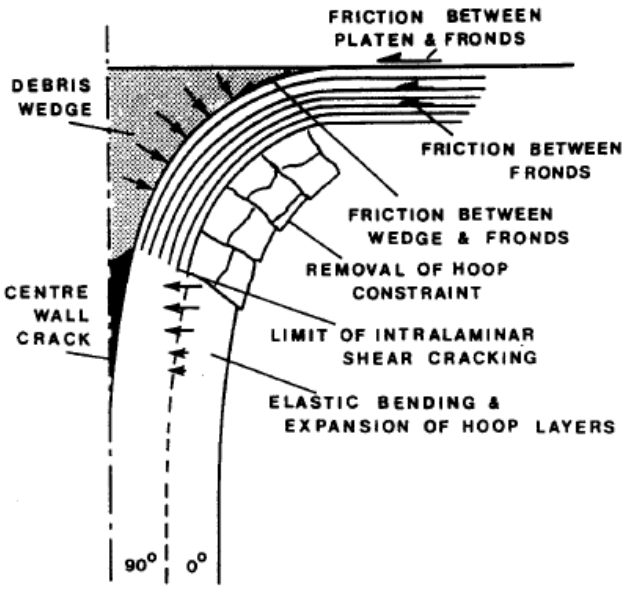

Fig. 13: Forces acting in the crush zone in splaying mode (90° denotes the axial direction of the tube) [24].

The behavior of the material and the development of these zones depends heavily on the orientation of the reinforcement fibers [1].

Fibers oriented in the axial direction (90°) are bent inwards or outwards as dictated by the constraints from neighboring fibers. Intralaminar cracks form normal to the fiber direction (the lamina splits into thinner layers), propagating through the weakest regions. Fibers in the hoop direction (0°) can expand outwards by fracturing or inwards by fracturing or buckling. The shear and tensile separation between the plies leads to delamination. The structure is made more resistant to crack propagation along the central region of the wall through the compressive stiffness of the internal layers and through tensile stiffness of the outer plies and the bond between plies [1].

Based on the model outlined above, the main sources of energy dissipation are the following:

- Intrawall crack propagation
- Fronds bending due to delamination between plies
- Axial splitting between fronds
- Flexural damage of individual plies due to small radius of curvature at the delamination limits
- Friction due to axial sliding between plies
- Frictional resistance to the penetration of the debris wedge
- Friction from the sliding of fronds across the platen [21, 22].

Fig. 13 shows a schematic of the crush zone and acting forces within, most of which are a result of the friction between the fronds, wedge and platen [24].

Fragmentation / transverse shearing

Fragmentation is characterized by short (less than laminate thickness) interlaminar, intralaminar and axial cracks [20]. The main failure mechanism is a result of shear stresses caused by a mixture of fiber fracture, matrix fracture, fiber buckling and interlaminar cracks [30]. Following failure, lamina pieces and fragments are forced inside and outside the tube and the process repeats itself with the remaining material.

The main energy absorption mechanism of this process is fiber and matrix fracture. As opposed to splaying, there are no fronds or debris wedge present to contribute to energy absorption through frictional effects [30].

Folding / local buckling

This failure mode is a characteristic of metal tubes and select ductile fiber reinforced composites. Failure is characterized by interlaminar and longitudinal cracking during hinge formation, with a possibility of fiber fracture on the tension side of the hinge [20].

The main benefit of this collapse mode is post-crush integrity as a result of either the matrix or fibers remaining relatively intact [30].

Brittle fracture

Brittle fracture is a combination of fiber splaying and fragmentation and includes the characteristics of both. It is also the most ideal in terms of absorbed energy out of the four stable collapse modes. The longitudinal cracks are long enough to form fronds, which are then bent through such a radius of curvature as to fracture. Compressive stresses cause the formation of a debris wedge which assists in the formation of fronds as it attempts to split the tube wall [30].

The energy absorption mechanisms present during this failure mode includes elements from both splaying and fragmentation, including fiber and matrix fracture, friction, frond bending and crack growth [30].

2.4. Material models for numerical simulations

The simulation of composite components is carried out in various FE solvers such as ANSYS, LS DYNA, ABAQUS, NASTRAN etc. The current study concerns analyses carried out in LS DYNA with the help of ANSA/META for pre- and postprocessing, which involves virtually replicating the boundary conditions of the physical testing and the evaluation of the results.

The most important aspect of the analysis is the material model of the CFRP composite material. A good starting point is required to iteratively change the parameters for the results to match those of the physical measurement. Since the simulated crushing process requires a material model with progressive material failure, MAT54 is commonly used. This material type enables the definition of orthotropic layers in composite shell structures and includes a damage model without excessive complexity. The model is only available inside LS DYNA.

A study by Feraboli et al [27] using this material model concluded that MAT 54 is suitable for simulating the crushing process in a sinusoidal specimen, albeit through calibration of the parameters by trial and error. The analysis is also highly sensitive to other parameters such as mesh sizing, contact definition, crush front softening parameter etc.

2.5. Summary of literature review and goals

Chapters 2.1 - 2.4 summarize the behavior and failure of composite materials both in a general sense and applied to the axial crushing load case. The topic had already been widely researched and the failure mechanisms are well documented, including their mechanisms, onset criteria and energy absorbing capabilities. The main goal when designing a composite energy absorbing structure is to ensure the stable and controlled collapse of the specimen with the highest possible value of specific energy absorption.

The current study aims to accomplish a similar goal: analyze the crushing behavior of composite specimens and define a set of materials to be used in numerical finite element simulations for the design of light crash structures. The stable crushing modes of the tested specimens will be assisted by a trigger mechanism and appropriate layup.

Defining material parameters for FEA will include the fitting of the simulation results to those of the tested specimen. The static properties of the material had previously been defined and will be used for this analysis. Dynamic properties will be adjusted in an iterative manner, refining their value after comparing the results of the simulation, limiting them to an essential set of parameters in order to avoid overcomplicating the process.

3. APPLIED MATERIALS AND INSTRUMENTS

3.1. Materials

3.1.1. Carbon fiber prepreg

The material used for this study was the T700S standard modulus carbon fiber prepreg from Toray Industries. The material's fiber content is 36% and is paired with an ER450 resin. The notable material properties include a tensile strength of 2550 MPa, a tensile modulus of 135 GPa and a compressive strength of 1470 MPa according to the datasheet from the manufacturer (Fig. A1 in the appendix).

3.2. Instruments

3.2.1. Zwick Z250 universal testing machine

The mechanical tests were carried out with a Zwick Z250 (Zwick GmbH & Co. KG, Ulm, Germany) material testing machine with a testing speed range of 0,001 - 600 mm/min and a maximum load of 250 kN. The tests were performed at a speed of 600 mm/min (10 mm/s) and a 250 kN load cell. The results were acquired using the Zwick TestXpert II 3.41 software and evaluated in Microsoft Excel.

3.2.2. Thermal imaging sensor

The thermal monitoring of the crushing process was done with a FLIR A325sc (Teledyne FLIR LLC, Wilsonville, Oregon, USA) camera and the accompanying FLIR ResearchIR software. The resolution of the camera is 320 px x 240 px, with the measurement accuracy within ± 2 K of the real value. The device was calibrated based on the temperature and humidity of the lab, in addition to the emissivity of the composite material and the measurement distance. The camera was part of the test setup as seen on Fig. 15.

3.2.3. High-speed camera

The high-speed camera used for the monitoring of the measurements was a Keyence VW-9000 (Keyence International, Mechelen, Belgium) with a resolution of 640 px x 480 px and a maximum recording speed of 230000 fps at 160 px x 32 px. The zoom lens used was a VW-Z5. The camera was part of the test setup as seen on Fig. 15.

4. DEVELOPMENT AND DESIGN

4.1. Crushing test of a composite tube

The crushing process was reproduced by the axial crushing of composite tube specimens. This load case with this geometry is the most widely researched and simplest way of obtaining data about the energy absorption characteristics of composite materials.

4.1.1. Specimen properties

The specimens were composite tubes (Fig. 14) with an inner diameter of 38 mm and a height of 100 mm. A chamfer was placed at the top of the specimen to act as the crushing trigger, which enables the stable crushing of the tube by preventing global buckling.

Fig. 14: Composite tube specimens

The layup consisted of four T700 UD plies with (90/0/0/90) layer orientations. The 0° direction denotes the axial direction, while 90° stands for the hoop direction. The 90° plies are meant to provide stability by constraining the 0° plies, provide the most significant portion of the energy absorption capability of the structure.

All four specimens were measured prior to testing, including their dimensions and weight. This data is needed to calculate the SEA of the structure.

4.1.2. Test setup

The tests were carried out on the Zwick Z250 universal testing machine at 10 mm/s, which was the highest speed available. Although crash events happen at considerably

higher speeds, this velocity was adequate for calibrating the material model. The specimen was placed on a flat surface and was axially loaded with a flat load applicator. The test setup is shown on Fig. 15.

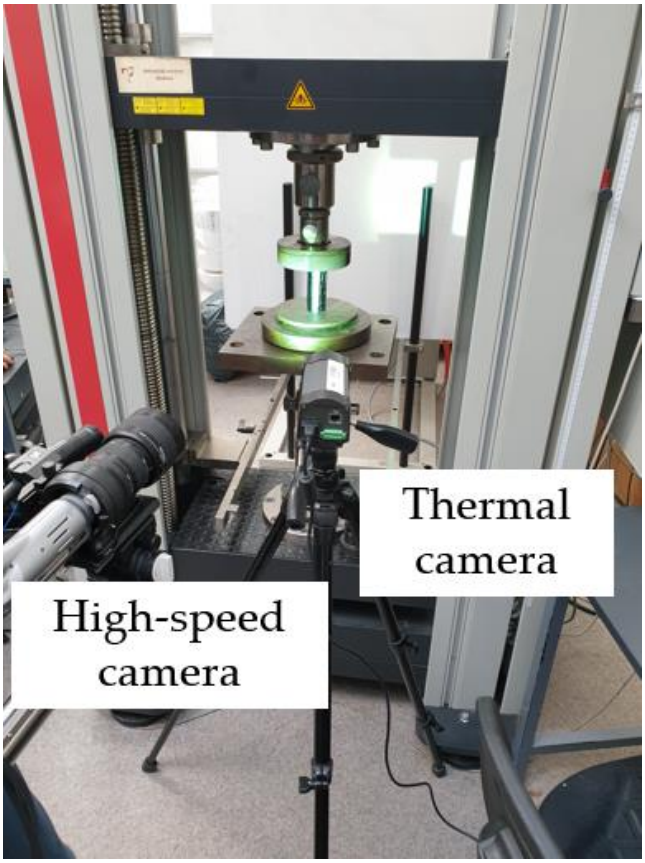

Fig. 15: Test setup

Additional observation techniques were employed, including a high-speed camera and a thermal imaging sensor. The former was used to capture the details of the crushing process, while the thermal camera provided additional information about the heat produced during the process.

4.1.3. Test results

The crushing process is showcased on Fig. 16 through images taken from the high-speed camera footage. The specimens with the layup (90/0/0/90) all exhibited crushing behavior during loading. A stable collapse was initiated, with the tubes gradually failing without buckling. Fiber splaying is observed along with fragmentation of the 0° plies.

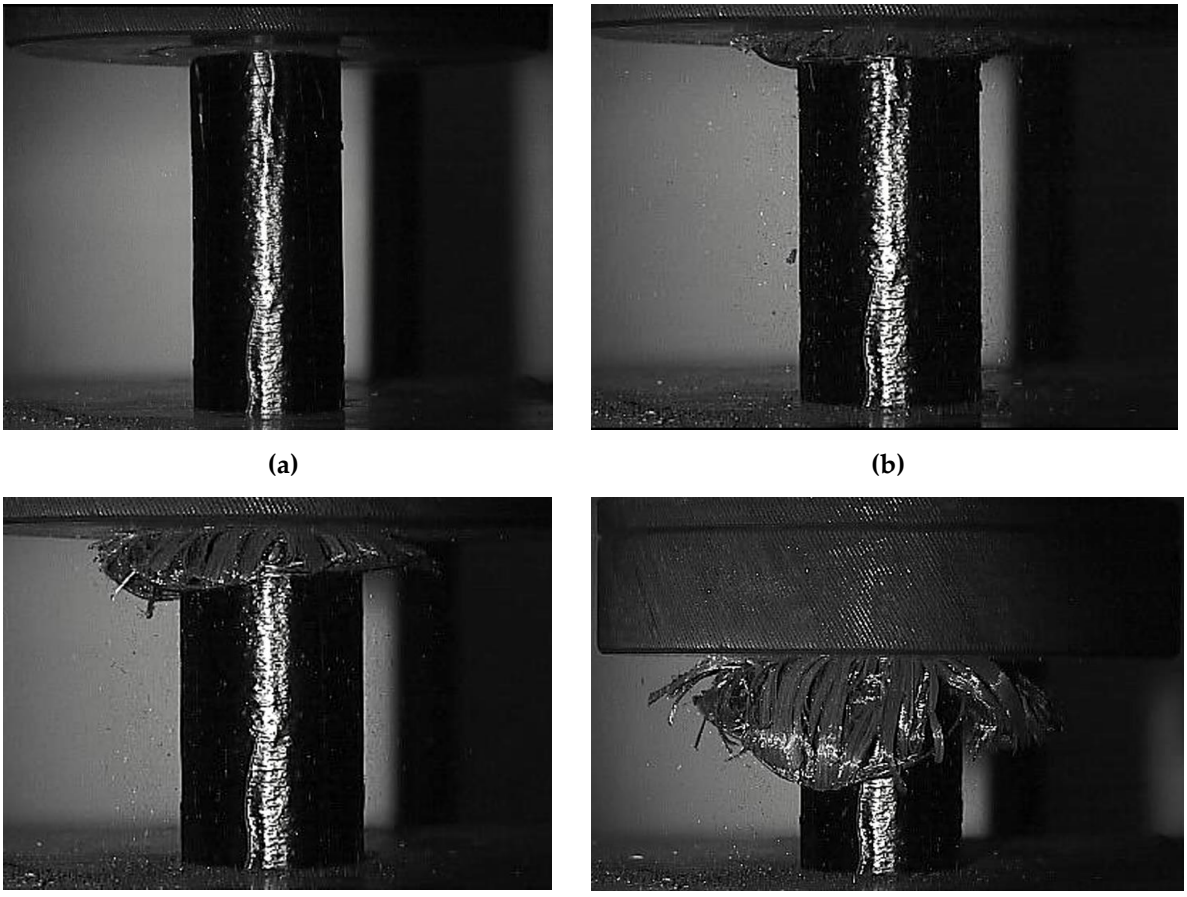

(a) **(b)**

(c) **(d)**

Fig. 16: Crushing process of the composite specimen from (a) through (d)

4.2. Recreation of the physical test through numerical simulation

The results of the crushing tests were recreated with numerical simulations in order to model the crushing characteristics of the material. The defined material properties can later be used to analyze the behavior of complex geometries without the need for physical testing.

4.2.1. Material parameters

The MAT54 material card provides many parameters to define both the conventional static behavior and the post-failure mechanisms of the structure. The parameters are sorted into groups based on which aspects they control (Fig. 17). There are numerous parameters which purely mathematical and thus not experimentally definable. These parameters are either damage factors which reduce various properties of the material following failure or deletion parameters which delete an element after reaching the specified value (most often strain). Constitutive and strength properties can be measured experimentally. To simplify the problem, only the parameters with the biggest effect on the crushing behavior were changed during

the optimization process. These parameters are marked with borders on Fig. 17. The modeling of cohesive interface layers between plies was considered but abandoned after several iterations as it complicated the simulation and added too many additional parameters to calibrate.

*MAT_054 (ENHANCED_COMPOSITE_DAMAGE): Pa, sec, m, kg/m^3							
mid	ro	ea	eb	ec	prba	prca	prcb
0	1500	1.5E11	1.5E10	1.5E10	0.0192	0.0192	0.4
gab	gbc	gca	kfail	aopt			
1.2E10	5,00E+09	1.2E10	0	0			
xp	yp	zp	a1	a2	a3	mangle	
0	0	0	0	0	0	0	
v1	v2	v3	d1	d2	d3	dfailm	dfails
0	0	0	0	0	0	0.55	
tfail	alph	soft	fbrt	ycfac	dfailt	dfailc	efs
2,00E-08	0	0	0	0	0.025	-0.07	0
xc	xt	yc	yt	sc	crit	beta	
-8,00E+09	7,00E+09	3,00E+09	3,00E+08	4,00E+08	0	0	

1. Constitutive properties: RO, EA, EB, EC, PRBA, PRCA, PRCB, GAB, GBC, GCA, KF

2. Local material axes: AOPT, XP, YP, ZP, A1-A3, MANGLE, V1-V3, D1-D3

3. Shear weighing factors: ALPH, BETA

4. Deletion parameters: DFAILM, DFAILS, TFAIL, DFAILT, DFAILC, EFS

5. Damage factors: SOFT, FBRT, YCFAC

6. Material strengths: XC, XT, YC, YT, SC

7. Failure criterion selection: CRIT

Fig. 17: Overview of MAT054 material card parameters

Longitudinal compressive strength (XC)

This parameter was primarily responsible for setting the initial load peak experienced when loading the specimen with higher values leading to a higher load peak. It did not have a noticeable influence on the post-crushing behavior of the structure.

Maximum strain for fiber tension and compression (DFAILT, DFAILC)

These parameters had arguably the biggest impact on the results, as they defined at which tensile/ compressive strain an element is deleted from the simulation and is no longer able to bear any load.

Low values of the compressive component (DFAILC) lead to global buckling with the tube failing at the bottom due to premature deletion, while raising the values too high leads to not enough elements being deleted and the instability of the simulation. The tensile component plays an important role in the behavior of the hoop fibers since they are forced inside/outside the structure and DFAILT defines when they are

deleted. Higher values lead to the elements remaining intact and being able to bear loads for longer.

Maximum strain for matrix tension and compression (DFAILM)

This parameter was used to stabilize the simulation. In case DFAILT and DFAILC failed in deleting enough failed elements, the accumulation of these distorted elements lead to instabilities and longer simulation run times. DFAILM can delete elements that experience failure in the tensile/compressive matrix direction instead of the fiber direction. Lowering this value could lead to elements being deleted ahead of the crush front or at the bottom of the tube.

Softening reduction factor (SOFT)

The SOFT factor defines the "softening" of the stiffness properties of elements at the crush front, which is defined as elements neighboring failed (deleted) elements. Its value should be less than 1 and defines what the stiffness properties of the elements are multiplied by following failure. This function helps avoid high load peaks and buckling due to the sudden loading of the entire cross section of the tube.

4.2.2. Geometry and meshing

The geometry was a shell tube with a diameter of 38 mm and a height of 100 mm. Using the part card TSHELL_LAMINATE, a 4-ply laminate with 0.3 mm thick layers was created. The elements were thick shells with a uniform sizing of 2 mm. The crushing trigger differed from the specimen: the simulation was the most stable when the two outside layers were left an element taller than the inside layers.

4.2.3. Boundary conditions

The loading plate was modeled with a plate placed at the top of the specimen, perpendicular to the axis of the tube. The plate was assigned the MAT20 material card, making it a non-deformable rigid body. A constant velocity of 10 m/s was applied in the axial direction of the specimen. The loading speed was increased from the physical measurement to reduce simulation time; the difference in results is minimal in the case of quasi-static loading. The loading plate itself was also the contact, modeled with the CONTACT_ENTITY card, which is a simple but effective contact formulation using a geometric entity instead of a meshed surface.

The nodes on the bottom surface of the specimen were constrained in all degrees of freedom to secure the structure.

4.2.4. *Control parameters*

The simulations ran for 0,005 seconds, allowing the loading plate to reach the half point of the original specimen height (50 mm). This distance was sufficient to evaluate the behavior of the tube, as the crushing load had stabilized before this point.

4.2.5. *Final material parameters*

Below are the results of the iterative parameter definition process. The simulation load curve accurately predicts the mean crushing load and the energy absorbed during the crushing process. The data shown on Fig. 18 was filtered with the 600 Hz SAE method.

To quantify the difference between the simulation and reality, the energy absorption values of the two scenarios were compared. The area under the load displacement curves was calculated up to 30 mm displacement since all measurements were performed to at least this value. The 30 mm displacement was measured from the point where the reaction force exceeded 1 N. This is necessary because the force reaction of the simulation is instantaneous, while the measurement curves noticeably lag behind due to the initial gap between the load applicator and the specimen.

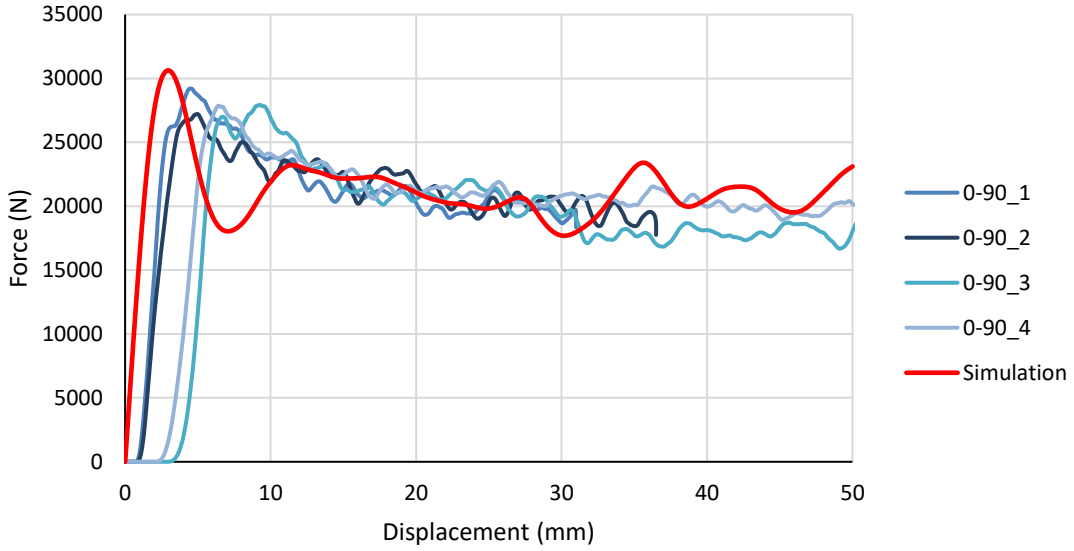

Fig 18: Load-displacement curves of the measured specimens and the simulation

The absorbed energy for each measurement and the simulation is displayed in Table 1.

Specimen	Absorbed energy (J)
0-90_1	644
0-90_2	641
0-90_3	619

0-90_4	631
Simulation	637

Table 1: Absorbed energy comparison between the measured specimens and the simulation

The average of the energy absorbed during physical testing is 634 ± 11 J, which makes the margin of error between the simulation and reality 0,5%.

Another important parameter to compare is the peak load, the results of which are summarized in Table 2.

Specimen	Peak load (N)
0-90_1	29202
0-90_2	27213
0-90_3	27936
0-90_4	27868
Simulation	30629

Table 2: Peak force comparison between the measured specimens and the simulation

The average in this case is 28055 ± 831 N, which means the simulation overestimates reality by 9,2%.

The list of the final material parameters which were iteratively changed during the process is found in the table below.

Parameter	Value
EA (Young's modulus in 1-direction)	150 GPa
EB (Young's modulus in 2-direction)	15 GPa
PRBA (minor Poisson's ratio)	0.0192
GAB (shear modulus)	12 GPa
XC (compressive strength in 1-direction)	-8 GPa
XT (tensile strength in 1-direction)	2 GPa
YC (compressive strength in 2-direction)	300 MPa
YT (tensile strength in 2-direction)	50 MPa
SC (shear strength)	400 MPa
DFAILT (maximum strain for fiber tension)	0.025
DFAILC (maximum strain for fiber compression)	-0.07
DFAILM (maximum matrix tensile/compressive strain)	0.55

Table 3: List of final material parameters

In conclusion, the parameters of a simulation model which can accurately predict the absorbed energy of an axially loaded composite tube with negligible deviation

from the physical measurement results were defined. This enables the setup of the simulation environment for the crash structure and the definition of the layup without the need for further physical testing.

4.3. Design of the crash structure

4.3.1. Requirements (Formula Student rulebook)

The Formula Student rulebook defines a set of constraints for the design of the crash structure, which are listed in Table A1 of the appendix. The rules which reference other subassemblies are omitted for the sake of clarity. The main requirements include the amount of energy absorbed by the structure (7350 J) and the geometrical constraints (minimum 200x100x100 mm). The physical testing conditions on which the simulations are based are also described in detail. The crash structure is named the Impact Attenuator and will be referred to as the IA from this point on.

4.3.2. Attachment of the IA to the chassis

The IA is attached to an anti-intrusion plate (from now: AIP), which is bolted to the chassis. The optimal solution for the attachment of the two parts is with the use of adhesives, which require no added parts (e.g bolted connection) and add minimal weight.

4.3.3. Manufacturing

Due to the geometry of the part (Chapter 4.3.4), the IA can be manufactured with a positive epoxy mold placed inside the hollow structure. The use of multi-part tooling is not necessary, and the geometry of the tool is simple which makes this a cost-effective solution.

4.3.4. Geometry and meshing

The geometry chosen for the impact structure is a square frustum. The edges of the structure were rounded in order to avoid stress concentrations. The geometry is rule compliant with the minimum dimension requirements and the front of the geometry was closed. This form was chosen as it is simple and is the easiest to manufacture. The geometry was meshed with 2 x 2 mm thick shell elements.

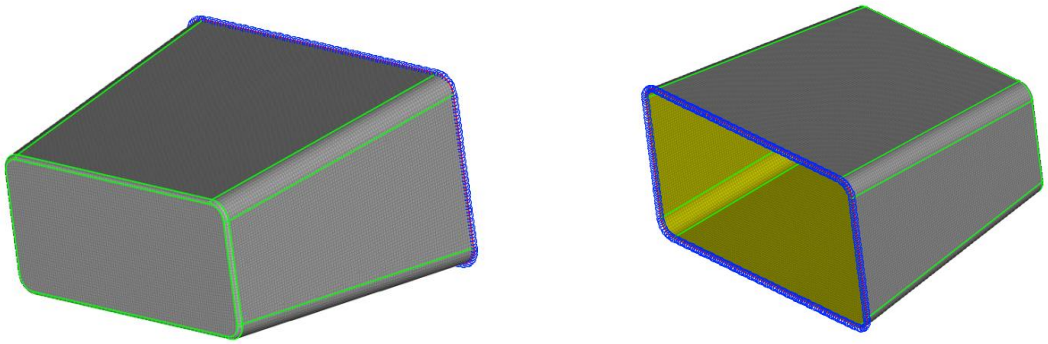

(a) (b)

Fig. 19: Meshed geometry of the IA including constrained nodes (attachment to AIP). Front (a) and rear (b) view

4.3.5. Layup

The layup chosen for the analysis was similar to that of the tested tube specimens: (90/0/0/0/0/0/90). More 0° plies were added to increase the crushing capability of the structure, while the core concept of applying 90° plies to support the inner and outer surfaces remained unchanged.

4.3.6. Boundary conditions

All nodes on the surface on which the Impact attenuator (later: IA) is attached to the chassis of the car were constrained in all degrees of freedom.

The RIGIDWALL card found in LS DYNA was responsible for the loading of the structure. This card enables assigning mass and initial velocity to a plane wall, which will then impact the IA. A mass of 300 kg and an initial velocity of 7 m/s was assigned to the rigid wall in accordance with rule T3.19.1 in Table 4.

4.3.7. Control parameters

The runtime of the simulation was defined based on previous drop-tower tests conducted with an aluminum honeycomb energy absorbing structure, which is the most commonly used in Formula Student. The time taken to decelerate the mass was about 0,04 s, so a value of 0,05 s was chosen as the termination time.

The parameters to be evaluated are the force-displacement curve and the mass acceleration/velocity plotted as a function of time. The rules define a minimum amount

of absorbed energy and a limit on the peak/average deceleration of the mass as a safety measure to protect the occupant in the event of a crash.

With the simulation environment already set up, the testing and design of multiple geometries and layup combinations is possible thanks to the defined material parameters. These simulations are currently in progress, the results will be presented at the conference.

SUMMARY

4.4. Summary in Hungarian

A szálerősítésű polimer kompozit anyagok széles körű elterjedtsége főként kiemelkedő fajlagos tulajdonságaiknak köszönhető. Ezek közé tartozik kiváló merevségük, szilárdságuk, valamint korrózió- és kifáradással szembeni ellenállásuk a legtöbb fémhez viszonyítva. Mindez lehetővé teszi, hogy olyan területeken váltsanak ki más anyagokat, ahol az alkatrészek tömege a legfőbb szempont, mint a motorsport, repülőgépipar vagy űripar. Maguk a szálerősítésű polimer kompozitok két fő komponensből állnak: az erősítő szálakból, mint szén, üveg, vagy aramid, illetve természetben megtalálható szálas anyagok; valamint a szálak közötti erőátvitelt biztosító mátrixanyagból, ami a legtöbb esetben egy térhálós polimer, mint az epoxi, vinilészter vagy poliészter.

Alkalmazási területeik között szerepel többek között az energiaelnyelő ütközőstruktúrák anyagának biztosítása. A hagyományos fém alapanyagú alkatrészekkel szemben nem képlékeny alakváltozáson keresztül nyelik el az energiát az erősítő szálak alakíthatóságának hiányában. Ehelyett a kompozitok leghatékonyabb energiaelnyelő mechanizmusa a megfelelően elindított összenyomás során végbemenő száltöredezés. Egy ennek megfelelően tervezett kompozit struktúra fajlagosan több energiát képes elnyelni, mint a fémből készült párja. Az elnyelt energia mértéke a geometria és anyagtulajdonságok mellett függ az összenyomást elindító folyamat megfelelő lefolyásától is, amely az egyik legfontosabb tervezési szempontnak mondható és emiatt kitüntetett figyelmet igényel.

Jelen kutatás célja egy frontális ütközőstruktúra tervezési feltételeinek megteremtése. A folyamat első részét képezte az egyszerű próbatest geometriákon végzett mérések szimulációs térben való előállítása, majd az eredmények reprodukálása az adott anyagparaméterek iteratív változtatásával. Az így behangolt paraméterekkel képes voltam a mérés eredményeit 0,5%-on belül megközelíteni. A tervezési folyamat végső lépéseként a Formula Student szabályzatának megfelelő ütközőstruktúra geometriájának és rétegrendjének meghatározása következett ezeknek az anyagtulajdonságoknak a felhasználásával.

4.5. Future improvements

The prediction and characterization of the crush behavior of composites could be improved by several means. First, using a different material model inside LS DYNA with more detailed degradation and failure characteristics (e.g. continuum damage models) could lead to more accurate results. This would also require extensive material testing. Furthermore, conducting tests with multiple load cases e.g. off-axis impact, drop tower testing could provide a better picture of material characteristics outside of quasi-static axial crushing. Real structures are often subjected to multi-axial

loading which necessitates the characterization of the material properties under these circumstances.

5. REFERENCES

[1] Mamalis A. G, Robinson M., Manolakos D. E., Demosthenous G. A., Ioannidis M. B., Carruthers J.: Crashworthy capability of composite material structures. Comp. Struct., **37**, 109-134 (1997).

[2] Mamalis, A. G., Manolakos, D. E., Demosthenous, G. A. and Ioannidis, M. B.: The static and dynamic collapse of fibreglass composite automotive frame rails. Comp. Struct., **34,** 77 (1996).

[3] Thornton P.H.: Energy absorption in composite structures. J. Comp. Mats, **13**, 247 (1979).

[4] Farley, G. L.: Energy absorption of composite materials. J. Comp. Mats, **17**, 167 (1983).

[5] Thornton P. H., Edwards P. J.: Energy absorption in composite tubes. J. Comp. Mats, **16**, 521 (1992).

[6] Hamada H., Coppola J. C., Hull D., Mackawa Z., Sato H.: Comparison of energy absorption of carbon-epoxy and carbon-PEEK composite tubes. Composites, **23**, 245 (1992).

[7] Schmueser D. W., Wickliffe, L. E.: Impact energy absorption of continuous fiber composite tubes. J. Eng. Mat. Trans. ASME, **72**, 72 (1987).

[8] Mamalis A.G., Yuan Y. B., Viegelahn G. L.: Collapse of thin-wall composite sections subjected to high-speed axial loading. Int. J. Vehicle Design, **13**, 564 (1992).

[9] Farley G. L.: Effect of specimen geometry on the energy absorption of composite materials. J. Comp. Mats, **20**, 390 (1986).

[10] Mamalis A. G., Manolakos D. E., Viegelahn G. L.: Crashworthy behaviour of thin-walled tubes of fiberglass composite material subjected to axial loading. J. Comp. Mats, **24**, 72 (1990).

[11] Czaplicki M. J., Robertson R.E., Thorton P. H.: Comparison of bevel and tulip triggered pultruded tubes for energy absorption. Composites Science and Technology, **40**, 31 (1991).

[12] Mamalis A. G., Manolakos D. E., Demosthenous G. A., Ioannidis M. B.: Axial collapse of thin-walled fiberglass composite tubular components at elevated strain-rates. Composites Engineering, **3**, 653 (1990).

[13] Mamalis, A. G., Manolakos, D. E., Demosthenous, G. A., Ioannidis, M. B.: Energy absorption capability of fibreglass composite square frusta subjected to static and dynamic axial collapse. Thin-Walled Structures, **25**, 269 (1996).

[14] Mamalis, A. G., Manolakos, D. E., Viegelahn, G. L., Demosthenous, G. A., Yap, S. M.: On the axial crumpling of fibre-reinforced composite thin-walled conical shells. Int. J. of Vehicle Design, **12**, 450 (1991).

[15] Mamalis, A. G., Manolakos, D. E., Viegelahn, G. L., Yap, S. M., Demosthenous, G. A.: Microscopic failure of thin-walled fibre-reinforced composite frusta under static axial collapse. Int. J. Vehicle Design, **12**, 557 (1991).

[16] Farley, G. L., Jones, R. M.: Crushing characteristics of composite tubes with 'near-elliptical' cross sections. J. Comp. Mats, **26**, 1252 (1992).

[17] Farley G. L.: The effect of crushing speed on the energy-absorption capability of composite tubes. J. Comp. Mats, **25**, 1314 (1991).

[18] Kindervater C. M.: Energy absorption of composites as an aspect of aircraft structural crash resistance. Developments in the Science and technology of Composite Materials, 643 (1990).

[19] Savage G.: Safety and survivability in Formula One motor racing. Metals and Materials, 147 (1992).

[20] Farley G. L., Jones L. M.: Crushing characteristics of continuous fibre-reinforced composite tubes. J. Comp. Mats, **26**, 37 (1992).

[21] Fairfull A. H., Hull D.: Energy absorption of polymer matrix composite structures: Friction effects. Structural Failure for International Symposium on Structural Failure. 255, MIT (1988).

[22] Mamalis A.G., Manolakos D.E., Demosthenous G. A., Ioannidis M. B.: Analysis of failure mechanisms observed in axial collapse of thin-walled circular fiberglass composite tubes. Thin-Walled Structures, **24**, 335 (1996).

[23] Taljera R., Varna J.: Modeling Damage, Fatigue and Failure of Composite Materials. Woodhead Publishing, Cambridge (2016).

[24] Hull D.: A unified approach to the crushing of Fibre-Reinforced Composite Tubes. Composites Science and Technology, **40**, 377-421 (1991).

[25] Guohoa Z., Guangyong S., Hang Y., Shunfeng L., Qing L.: Energy absorption of metal, composite and metal/composite hybrid structures under oblique crushing loading. Int. J. Mechanical Sciences, **135**, 458-483 (2018).

[26] Mamalis A. G., Manolakos D. E., Demosthenous G. A., Ioannidis M. B.: On the bending of automotive fibre-reinforced composite thin-walled structures. Composites, **25**, 47 (1994).

[27] Feraboli P., Wade B., Deleo F., Rassaian M., Higgins M., Byar A.: LS-DYNA MAT54 modeling of the axial crushing of a composite tape sinusoidal specimen. Composites: Part A, **42**, 1809-1825 (2011).

[28] Tartaglione A.: Numerical simulation of adhesive joints under impact loading conditions. Politecnico di Torino (2021).

[29] LS DYNA Keyword User's Manual Volume II, Material Models. Livermore Software Technology (LST) (2021).

[30] Starbuck M. J., Adams D. O., Courteau M.: Energy Absorbing Damage Mechanisms in Progressive Crushing of Composite Tubes. Americal Society of Composites 32nd Technical Conference, West Lafayette (2017).

[31] Ramakrishna S., Hamada H.: Energy absorption characteristics of crash worthy composite materials. Key Engineering Materials, **141-143**, 585-620 (1998).

[32] Carruthers J. J., Kettle A. P., Robinson A. M., Energy absorption capability and crashworthiness of composite material structures: A review. Applied Mechanics Review, **51**, 635-649 (1998).

[33] Aoki R., Higuchi R., Yokozeki T., Aoki K., Uchiyama S., Ogasawara T.: Damage-mechanics mesoscale modeling of composite laminates considering diffuse and discrete ply damages: Effects of ply thickness. Composite Structures, **277** (2021).

[34] Gholizadeh S.: A review of impact behaviour in composite materials. International Journal of Mechanical and Production Engineering, **7**, 2321-2071 (2019).

6. APPENDIX

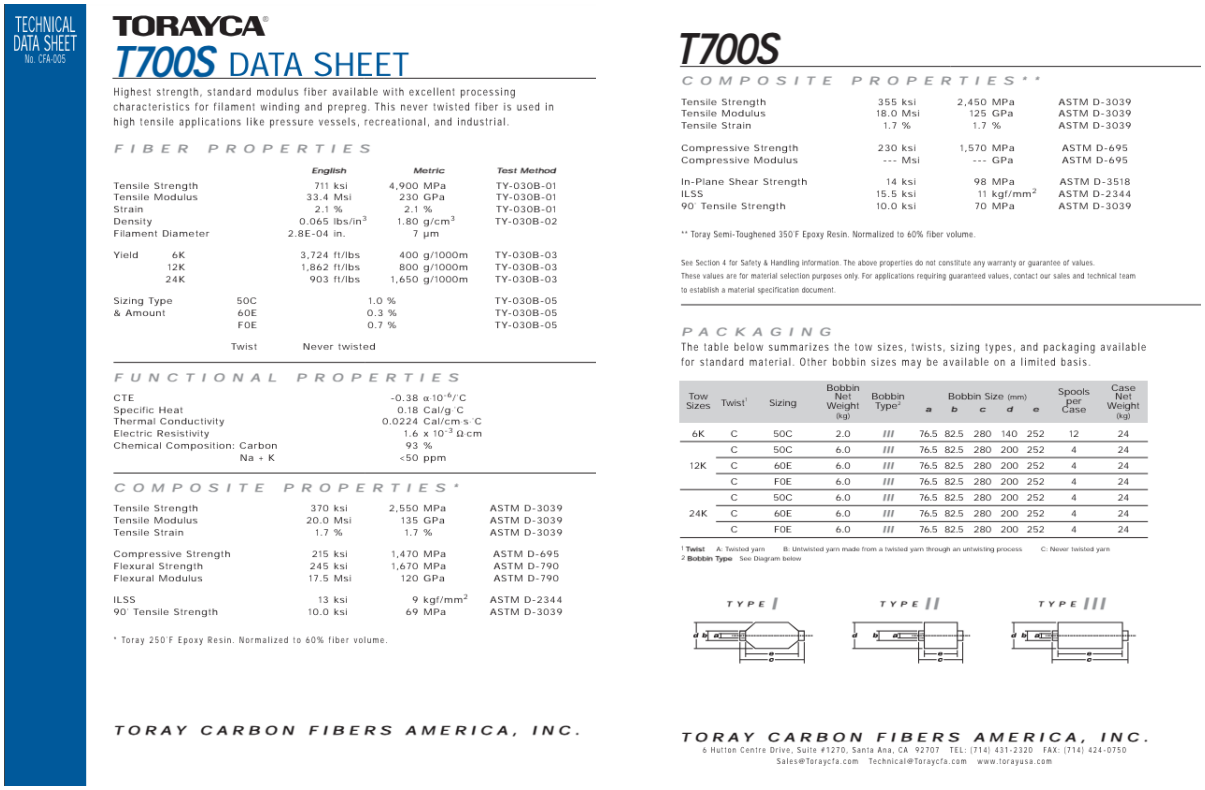

TECHNICAL DATA SHEET
No. CFA-005

TORAYCA®

T700S DATA SHEET

Highest strength, standard modulus fiber available with excellent processing characteristics for filament winding and prepreg. This never twisted fiber is used in high tensile applications like pressure vessels, recreational, and industrial.

FIBER PROPERTIES

		English	Metric	Test Method
Tensile Strength		711 ksi	4,900 MPa	TY-030B-01
Tensile Modulus		33.4 Msi	230 GPa	TY-030B-01
Strain		2.1 %	2.1 %	TY-030B-01
Density		0.065 lbs/in^3	1.80 g/cm^3	TY-030B-02
Filament Diameter		2.8E-04 in.	7 µm	
Yield	6K	3,724 ft/lbs	400 g/1000m	TY-030B-03
	12K	1,862 ft/lbs	800 g/1000m	TY-030B-03
	24K	903 ft/lbs	1,650 g/1000m	TY-030B-03
Sizing Type & Amount	50C	1.0 %		TY-030B-05
	60E	0.3 %		TY-030B-05
	F0E	0.7 %		TY-030B-05
	Twist	Never twisted		

FUNCTIONAL PROPERTIES

CTE	-0.38 $\alpha 10^{-6}$/°C
Specific Heat	0.18 Cal/g·°C
Thermal Conductivity	0.0224 Cal/cm·s·°C
Electric Resistivity	1.6 x 10^{-3} Ω·cm
Chemical Composition: Carbon	93 %
Na + K	<50 ppm

COMPOSITE PROPERTIES*

Tensile Strength	370 ksi	2,550 MPa	ASTM D-3039
Tensile Modulus	20.0 Msi	135 GPa	ASTM D-3039
Tensile Strain	1.7 %	1.7 %	ASTM D-3039
Compressive Strength	215 ksi	1,470 MPa	ASTM D-695
Flexural Strength	245 ksi	1,670 MPa	ASTM D-790
Flexural Modulus	17.5 Msi	120 GPa	ASTM D-790
ILSS	13 ksi	9 kgf/mm^2	ASTM D-2344
90° Tensile Strength	10.0 ksi	69 MPa	ASTM D-3039

* Toray 250°F Epoxy Resin. Normalized to 60% fiber volume.

TORAY CARBON FIBERS AMERICA, INC.

T700S

COMPOSITE PROPERTIES**

Tensile Strength	355 ksi	2,450 MPa	ASTM D-3039
Tensile Modulus	18.0 Msi	125 GPa	ASTM D-3039
Tensile Strain	1.7 %	1.7 %	ASTM D-3039
Compressive Strength	230 ksi	1,570 MPa	ASTM D-695
Compressive Modulus	--- Msi	--- GPa	ASTM D-695
In-Plane Shear Strength	14 ksi	98 MPa	ASTM D-3518
ILSS	15.5 ksi	11 kgf/mm^2	ASTM D-2344
90° Tensile Strength	10.0 ksi	70 MPa	ASTM D-3039

** Toray Semi-Toughened 350°F Epoxy Resin. Normalized to 60% fiber volume.

See Section 4 for Safety & Handling information. The above properties do not constitute any warranty or guarantee of values. These values are for material selection purposes only. For applications requiring guaranteed values, contact our sales and technical team to establish a material specification document.

PACKAGING

The table below summarizes the tow sizes, twists, sizing types, and packaging available for standard material. Other bobbin sizes may be available on a limited basis.

Tow Sizes	Twist[1]	Sizing	Bobbin Net Weight (kg)	Bobbin Type[2]	Bobbin Size (mm) a	b	c	d	e	Spools per Case	Case Net Weight (kg)
6K	C	50C	2.0	III	76.5	82.5	280	140	252	12	24
12K	C	50C	6.0	III	76.5	82.5	280	200	252	4	24
	C	60E	6.0	III	76.5	82.5	280	200	252	4	24
	C	F0E	6.0	III	76.5	82.5	280	200	252	4	24
24K	C	50C	6.0	III	76.5	82.5	280	200	252	4	24
	C	60E	6.0	III	76.5	82.5	280	200	252	4	24
	C	F0E	6.0	III	76.5	82.5	280	200	252	4	24

[1] **Twist** A: Twisted yarn B: Untwisted yarn made from a twisted yarn through an untwisting process C: Never twisted yarn
[2] **Bobbin Type** See Diagram below

TYPE I TYPE II TYPE III

TORAY CARBON FIBERS AMERICA, INC.
6 Hutton Centre Drive, Suite #1270, Santa Ana, CA 92707 TEL: (714) 431-2320 FAX: (714) 424-0750
Sales@Toraycfa.com Technical@Toraycfa.com www.torayusa.com

Fig. A1: Fiber and composite properties of T700S carbon fiber

Rule ID	Rule details
T1.1.6	Impact Attenuator (IA) – A deformable, energy absorbing device located forward of the front bulkhead.
T 3.17.1	Each vehicle must be equipped with an IA assembly consisting of an IA and AIP.
T3.17.2	The IA must be installed forward of the front bulkhead.
T3.17.2	The IA must be at least 100mm high and 200mm wide for a minimum distance of 200mm forward of the front bulkhead.
T3.17.2	No portion of the required 100x200x200 mm3 volume of the IA can be positioned more than 350mm above the ground.
T3.17.2	The IA must be not able to penetrate the front bulkhead in the event of an impact
T3.17.2	The IA must be attached securely and directly to the Anti Intrusion Plate (AIP).
T3.17.2	The IA must not be part of the non-structural bodywork.
T3.17.2	The IA must be designed with a closed front section.
T3.17.6	The attachment of the IA assembly must be designed to provide an adequate load path for transverse and vertical loads in the event of off-center and off-axis impacts. Segmented foam attenuators must have the segments bonded together to prevent sliding or parallelogramme.
T3.19.1	The IA assembly, when mounted on the front of a vehicle with a total mass of 300 kg and impacting a solid, non-yielding impact barrier with a velocity of impact of 7 m/s, must meet the following requirements:
T3.19.1	Decelerate the vehicle at a rate not exceeding 20 g average and 40 g peak
T3.19.1	The energy absorbed in this event must meet or exceed 7350 J.
T3.19.1	Equivalent (higher) test velocities are only allowed to accommodate for a lower testing mass, as long as the energy absorbed is 7350 J or more. If these requirements cannot be met, a team must use the standard IA::
T3.19.2	During the IA test:
T3.19.2	There must be at least 50 mm clearance rearwards of the AIP to the test fixture

T3.19.2	No part of the AIP may permanently deflect more than 25 mm beyond the position of the AIP before the test.
T3.19.3	Teams using IAs (typically structural noses) directly attached to the front bulkhead, which shortcut the load path through the bulk of the AIP, must conduct an additional test. This test must prove that the AIP can withstand a load of 120 kN (300 kg multiplied by 40 g), where the load applicator matches the minimum IA dimensions.
T3.19.5	Dynamic testing (sled, pendulum, drop tower, etc) of the IA may only be conducted at a dedicated test facility. This facility may be part of the university but must be supervised by professional staff. Teams are not allowed to design their own dynamic test apparatus
T3.19.6	When using acceleration data from the dynamic test, the average deceleration must be calculated based on the raw unfiltered data. If peaks above the 40 g limit are present in the data, a 100 Hz, 3rd order, low pass Butterworth (-3 dB at 100 Hz) filter may be applied.

Table A1: Impact attenuator design requirements